# A Simple Moment Method of Forest Biomass Estimation From Non-Gaussian Texture Information by High-Resolution Polarimetric SAR

Haipeng Wang, *Member, IEEE*, and Kazuo Ouchi, *Senior Member, IEEE*

***Abstract*—A simple method is described to estimate forest biomass by high-resolution polarimetric synthetic aperture radar (SAR). The method is based on the regression analysis between the measured biomass from the ground survey and the second intensity moment of the non-Gaussian texture in the cross-polarized L-band SAR images. The SAR data used in the analysis were acquired by the airborne polarimetric interferometric SAR over the coniferous forest in Hokkaido, Japan. The regression analysis was first carried out, and a model function was derived to relate the intensity moment and the measured biomass in 19 forest stands. Using this model function, the biomass values were estimated and compared with those of 21 different stands with known biomass. The average accuracy of the moment model was found to be 85%, which is similar to that of the previous $K$-distribution model. The advantage of this method over the distribution-based model is that there is no need to search a specific distribution function which fits best to the image texture.**

***Index Terms*—Forest biomass, intensity moment, non-Gaussian texture, polarimetric high-resolution data, synthetic aperture radar (SAR).**

## I. Introduction

THE IMPACT of forests on global warming is an important factor since the effective carbon dioxide ($CO_2$) release by the reduction of forests is considered as large as 20% of the total $CO_2$ release by fossil fuel burning [1]. Because of vast nature of forests, it is time consuming and labor intensive to measure forest parameters from ground, and therefore, the remotely sensed data, in particular, by synthetic aperture radar (SAR), have been used to estimate forest parameters. There are substantial numbers of reports regarding the retrieval of tree biomass by SAR, most of which are based on the relation between the backscatter radar cross section (RCS) and the biomass measured on site [2]–[12], although data fusion [13] and interferometric approaches [14] have also been reported. A different approach has also been proposed to estimate tree biomass [15], [16], utilizing the non-Gaussian texture patterns in high-resolution polarimetric SAR images of forests. In this method, a probability density function (pdf) which fits best to the image amplitude is sought, and an empirical model function is derived to describe a parameter of the pdf and the "ground-truth" biomass. For the Tomakomai national forests in Hokkaido, Japan, the $K$-distribution [17]–[19] was found to fit best to the cross-polarized images of coniferous forests acquired by the airborne L-band polarimetric interferometric SAR (Pi-SAR) [20]. The results showed that the $K$-distribution model could estimate the tree biomass beyond the saturation limits (approximately 40 tons/ha for the present study) of the RCS method with the average accuracy of approximately 86% for individual stands [15]. There are advantages and disadvantages in these two methods. The RCS method is simple and accurate but requires strict radiometric calibration. The other main drawback of the RCS method is that its saturation limits depend on many factors, including both SAR system parameters, such as incidence angle, wavelength, etc., and forest species [4], [9], [14]. The $K$-distribution model can estimate larger biomass with similar accuracy in comparison with the RCS method but requires a more complex procedure of finding a pdf which fits best to the data.

In this letter, a simple moment-based regression model without using a pdf is described. In this method, a regression model function was first derived to describe the relation between the second intensity moment (variance) and the ground-truth biomass of 19 stands in the same data used in the previous studies [15], [16]. From the model function, the biomass values of other 21 stands were estimated from the SAR data and compared with the ground-truth biomass. Clear advantages of this approach are that no specific pdf needs to be assumed and that no such strict radiometric calibration as that for the RCS method is required. It should be noted that the use of texture analysis for image classification and biomass estimation has been suggested in some previous papers [17], [21]–[25], but the quantitative empirical relation between the ground-truth biomass and the second intensity moment has not yet been reported.

In the next section, the Pi-SAR data and test sites, including the measured biomass, are briefly described, followed by the

Manuscript received December 3, 2009; revised February 9, 2010 and March 14, 2010. Date of publication May 27, 2010; date of current version October 13, 2010. This work was supported in part by the Pi-SAR Project jointly carried out by the National Defense Academy of Japan and Fudan University of China, by the Science Research Foundation for the Returned Overseas Chinese Scholars, State Education Ministry of China, and by the National Natural Science Foundation of China under Grants 40901201 and 60971091.

H. Wang is with the Key Laboratory of Wave Scattering and Remote Sensing Information, Department of Communication Science and Engineering, School of Information Science and Engineering, Fudan University, Shanghai 200433, China (e-mail: hpwang@fudan.edu.cn).

K. Ouchi is with the Department of Computer Science, School of Electrical and Computer Engineering, National Defense Academy, Yokosuka 239-8686, Japan (e-mail: ouchi@nda.ac.jp).

Color versions of one or more of the figures in this paper are available online at http://ieeexplore.ieee.org.

Digital Object Identifier 10.1109/LGRS.2010.2047839

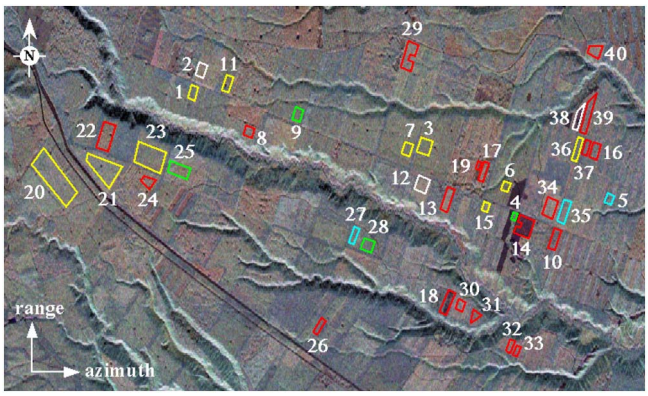


Fig. 1. Color composite Pi-SAR L-band polarimetric image of the Tomakomai national forest in Hokkaido, Japan. The HH-, HV-, and VV-polarization images correspond to red, green, and blue colors, respectively. The field measurements were made at the stands labeled from 1 to 40. The white, red, yellow, green, and blue colors of the stands represent the dominant tree species, corresponding to spruce, red pine, larch, Todo fir, and conifer of mixed species, respectively. Further details are shown in Table I.

regression analysis to derive a model function from the data of 19 stands. The model accuracy is then examined by comparison of the model-based biomass with the ground-truth biomass of other 21 stands. Finally, the updated regression model function is derived using all 40 sets of data, and a map of tree biomass around the test forests is produced using the updated model function as an example.

## II. SAR and Forest Data

The SAR data were collected by the airborne Pi-SAR [20]. The Pi-SAR is equipped with two quad-polarization X-band (9.55 GHz) antennas developed by the National Institute of Information and Communications Technology and a single quad-polarization L-band (1.27 GHz) antenna developed by the Japan Aerospace Exploration Agency (JAXA). The nominal spatial resolutions in a full single look are 0.375 m in the azimuth direction and 1.5 m in the range direction at X-band, and at L-band, they are 0.75 and 3 m in the respective directions.

The four-look Pi-SAR L-band image of the experimental site in the Tomakomai national forests is shown in Fig. 1. The scene center is at $(42°44' \text{ N}, 141°30' \text{ E})$, and the data were acquired on November 7, 2002. The image sizes are 8.9 km in the azimuth (from left to right) direction and 4.3 km in the range (from bottom to top) direction. The incidence angles are 38.4°, 44.1°, and 48.6° at the near range, center, and far range, respectively. For the regression analysis, full-single-look L-band polarization images were used.

The field measurements were made on the 40 stands indicated in Fig. 1, where the measurements of the stands 1 to 12 were made in November 2002, those of the stands 13 to 19 in August 2003, and those of the stands 20 to 40 in August and September 2005. During the field survey, the ground-truth data were collected, including tree species, height, diameter at breast height, basal area (tree cross section per unit area), and also soil moisture on a sample site on each stand. By using these data, the aboveground biomass was computed using the conversion formulas which are provided by the forestry management [15], [26]. The dominant species and the measured biomass are shown in Table I. The details of the field measurements and conversion from tree height and diameter to biomass are not repeated here since they are described in our previous paper [15].

TABLE I
Dominant Tree Species and Average Biomass of 40 Stands. The Biomass Is in the Unit of Tons per Hectare, and the Numbers in Brackets Are the Percentage of Dominant Species, Where the Term "Conifer" Implies a Stand of More Than Two Mixed Species. The Percentage Is the Ratio of the Biomass of the Dominant Species to the Total Biomass of All Species at Each Stand

| stands | tree species | $B$ | stands | tree species | $B$ |
|---|---|---|---|---|---|
| 1 | larch (75.4) | 83.7 | 21 | larch (74.7) | 107.8 |
| 2 | spruce (97.9) | 64.2 | 22 | red pine (93.7) | 85.6 |
| 3 | larch (86.0) | 57.2 | 23 | larch (75.2) | 111.8 |
| 4 | Todo fir (55.2) | 40.5 | 24 | red pine (81.8) | 71.9 |
| 5 | conifer | 47.6 | 25 | Todo fir (66.7) | 43.8 |
| 6 | larch (83.4) | 65.2 | 26 | red pine (52.0) | 67.5 |
| 7 | larch (95.9) | 83.6 | 27 | conifer | 71.6 |
| 8 | red pine (94.2) | 84.4 | 28 | Todo fir (48.1) | 79.6 |
| 9 | Todo fir (90.0) | 83.5 | 29 | red pine (86.8) | 126.7 |
| 10 | red pine (63.9) | 34.0 | 30 | red pine (83.5) | 97.5 |
| 11 | larch (94.0) | 57.4 | 31 | red pine (100.0) | 36.5 |
| 12 | spruce (98.0) | 70.4 | 32 | red pine (92.2) | 79.3 |
| 13 | red pine (73.3) | 99.5 | 33 | red pine (62.6) | 97.2 |
| 14 | red pine (100.0) | 0.9 | 34 | red pine (79.4) | 97.4 |
| 15 | larch (72.2) | 40.1 | 35 | conifer | 52.4 |
| 16 | red pine (89.9) | 66.7 | 36 | larch (46.8) | 121.0 |
| 17 | red pine (100.0) | 30.5 | 37 | red pine (59.0) | 66.8 |
| 18 | red pine (100.0) | 5.1 | 38 | spruce (100.0) | 0.1 |
| 19 | red pine (100.0) | 13.4 | 39 | red pine (89.9) | 56.9 |
| 20 | larch (64.7) | 50.8 | 40 | red pine (96.1) | 125.3 |

## III. Regression Analysis

### A. Second Intensity Moment and Biomass

For spaceborne SARs of intermediate resolution (20 × 20 m, for example), structures of scattering objects in the subresolution scale may not be resolved so that the resultant images appear as a granular intensity pattern known as Gaussian speckle. The Gaussian speckle does not carry information on the scattering objects except that there are many (more than four to eight) randomly distributed elementary scatterers within a resolution cell. However, high-resolution SARs such as Pi-SAR can resolve some features of scattering objects. Then, the image appears as "textured," which cannot be described by Gaussian statistics. Because the textural information depends on the scattering objects, the parameters on the objects can be extracted from the non-Gaussian properties of image amplitude fluctuations. This is the basis of the pdf-based regression model [15], [16] utilizing strong correlation between the order parameter of the $K$-distribution pdf, and tree biomass was developed.

In addition to the distribution function, the non-Gaussian property can also be characterized by the moment (variance) of image intensity or amplitude. In general, the second intensity moment of the non-Gaussian speckle increases with increasing non-Gaussianity from the value of two of the Gaussian speckle. It is this second intensity moment that we use for estimating the tree biomass. In the present study, we first examine the correlation between the second intensity moment of Pi-SAR images of the stands labeled 1 to 19 in Fig. 1 and the

ground-truth biomass listed in Table I. The second intensity moment can be computed from

$$\frac{\langle I^2\rangle}{\langle I\rangle^2} = \frac{1}{N}\sum_{j=1}^{N} I_j^2 \Bigg/ \left(\frac{1}{N}\sum_{j=1}^{N} I_j\right)^2 \tag{1}$$

where the angular brackets indicate an ensemble average, $I$ is the image intensity, $I_j$ is the $j$th pixel (intensity) value, and $N$ is the total number of pixels within the image of a stand. The size of the stands in the Tomakomai forests was typically 500 $\times$ 500 m, and some stands were subdivided further into smaller sizes. The intensity moment is computed over a comparably flat area of each stand, avoiding the areas such as rivers and areas without trees which yield statistically nonstationary texture. The number of pixels depends on the image size of a stand, ranging from 2874 to 22 868. Statistical stationarity and ergodicity are assumed so that the ensemble average is approximated by the sample average. The confidence level of the estimated intensity moment can be computed from the variance $\sigma_M^2$ of (1) as [17]

$$\sigma_M^2 \simeq \frac{1}{N}\left(\frac{\langle I^4\rangle}{\langle I\rangle^4} - \frac{4\langle I^3\rangle\langle I^2\rangle}{\langle I\rangle^5} + \frac{4\langle I^2\rangle^3}{\langle I\rangle^6} - \frac{\langle I^2\rangle^2}{\langle I\rangle^4}\right). \tag{2}$$

The result of the regression analysis is shown in Fig. 2. The third-order polynomial

$$\frac{\langle I^2\rangle}{\langle I\rangle^2} = a_0 + a_1 B_m + a_2 B_m^2 + a_3 B_m^3 \tag{3}$$

was used for the regression curve, where $B_m$ is the biomass by field measurement. The coefficients of the HH-, VV-, and HV-polarization data were found to be $a_0 = (2.480, 2.236, 2.564)$, $a_1 = (-0.004, 0.007, -0.009)$, $a_2 = (4.598, -1.939, 6.414) \times 10^{-5}$, and $a_3 = (-3.723, 11.798, -1.851) \times 10^{-7}$; the correlation coefficient is $r = (-0.692, -0.692, -0.929)$, where the values inside the parentheses correspond to (HH, VV, HV). It can be seen that the cross-polarization data have the highest (absolute) correlation value than the copolarization data, which is similar to that of the $K$-distribution model [16]. Thus, the regression model of the cross-correlation data can be considered as a suitable model for biomass inversion.

The reason for increasing the second intensity moment with decreasing biomass is associated with the change in non-Gaussianity, which is similar to that explained in the previous paper [15]. Briefly, for dense forests with very large biomass, the backscattered field is modeled as a statistically white random field, and the resultant image is just a Gaussian speckle pattern. SAR images of dense rain forests are good examples. The second intensity moment of such speckle patterns takes a constant value of two [17], [18]. This situation corresponds to the large biomass region in Fig. 2, where the second intensity moment approaches the value of two with increasing biomass.

In the reverse direction of decreasing biomass, trees tend to become sparsely distributed, and the image tends to contain the bright discrete images of individual trees. The image amplitude fluctuations then obey non-Gaussian statistics, and the intensity moment increases from the value of two of the Gaussian speckle pattern. This non-Gaussianity is possible because of the high-resolution Pi-SAR which can resolve certain structures of forests. As the biomass approaches zero, the surface becomes bare soil which, in general, has randomly varying surface roughness; the image again becomes Gaussian speckle in this limit, and the second intensity moment is expected to drop sharply toward the value of two. However, in the test site of Tomakomai forests, the stands of small biomass, including the stands 14, 18, and 38, were covered by young transplanted trees and low vegetation, i.e., they were not bare soil, and therefore, the intensity moment did not drop as the biomass closely approaches zero in the HH- and HV-polarization data in Fig. 2. On the contrary, the moment of the VV-polarization data

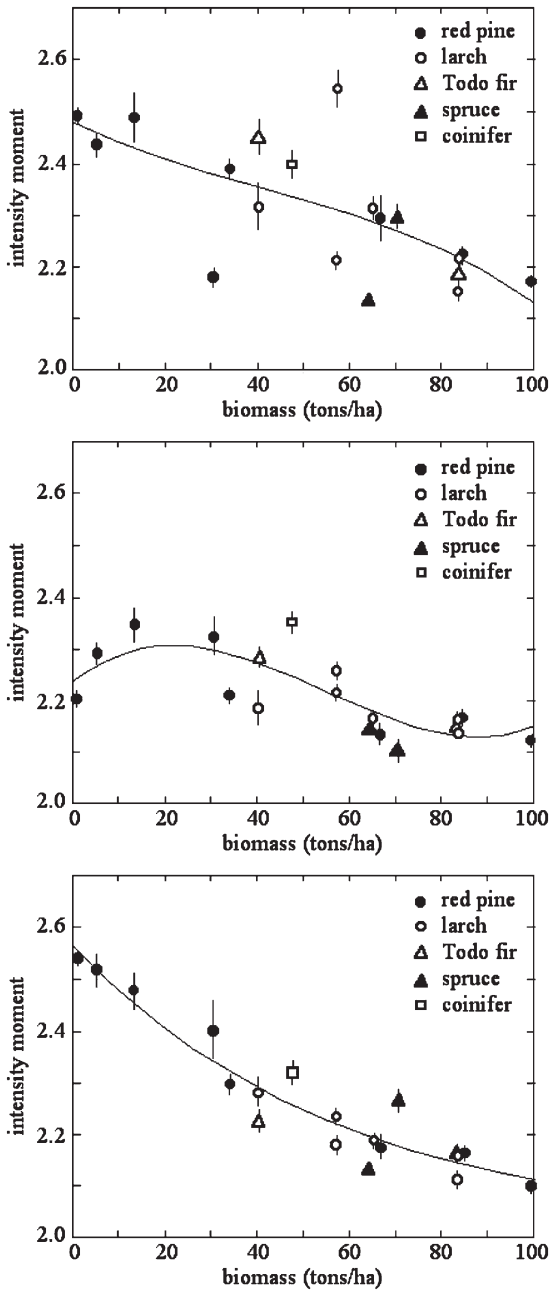


Fig. 2. (From top to bottom) Second intensity moment $\langle I^2\rangle/\langle I\rangle^2$ of the HH-, VV-, and HV-polarization images as a function of the tree biomass $B_m$ of stands 1–19.

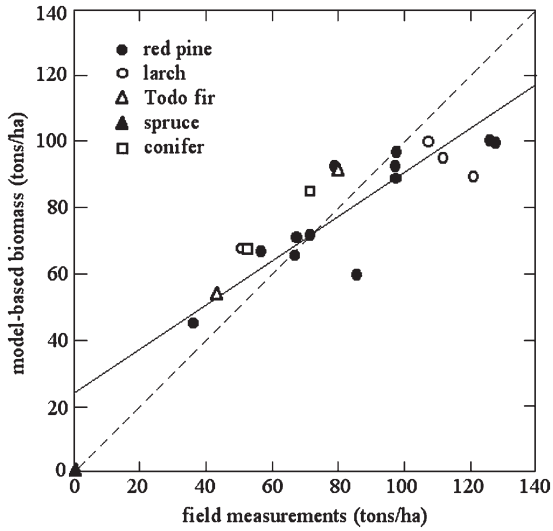


Fig. 3. Scatter diagram of the biomass estimated by the moment model and the ground-truth biomass of stands 20–40. The biomass values are listed in Table II. The solid line is the regression line fitted to the data, and the broken line shows the ideal relation.

decreases as the biomass approaches zero. The similar effect was seen in the VV-polarization data of the $K$-distribution model. The reason is not known and requires detailed numerical and experimental studies on the interaction between the incident microwave and forests. Such studies, however, are beyond the scope of this letter.

### *B. Comparison of Model-Based and Ground-Truth Biomass*

Having derived the regression model function of (3) for the HV-polarization data, the biomass values of the stands 20 to 40 were estimated using (3) and compared with the ground-truth biomass. Fig. 3 shows the scatter diagram between the model-based biomass and the ground-truth biomass, and the biomass values are shown in Table II. As can be seen in Fig. 3, good agreement is obtained with a correlation coefficient of 0.891, and the regression line is $B_{\text{model}} = 0.664 B_{\text{field}} + 23.903$. The average absolute accuracy was found to be approximately 85% for individual stands. This average accuracy is defined as $100 \times \sigma_M\%$, where

$$\sigma_M = 1 - \frac{1}{N}\sum_{j=1}^{N} \left| B_j^{(M)} - B_j \right| / B_j \tag{4}$$

and $B_j^{(M)}$ is the estimated biomass of the $j$th stand by the moment model, $B_j$ is the ground-truth biomass of the same stand, and the number of stands is $N = 21$ for the present case. It is of some interest that the root-mean-square error of the moment method is 19.4% of the average ground-measured biomass, corresponding to the biomass of 15.2 tons/ha.

### *C. Updated Model Function*

Fig. 4 shows the result of the regression analysis using all the biomass data of 40 stands. The coefficients of the model function are now $a_0 = 2.265$, $a_1 = -0.0126$, $a_2 = 1.097 \times 10^{-4}$, and $a_3 = -3.484 \times 10^{-7}$, and the correlation coefficient is $r = -0.863$. The biomass saturation starts from approximately 80–100 tons/ha, and these values may be the upper limit of biomass estimation by the moment model. Using this model function, a biomass map surrounding the test site forests was produced, as shown in Fig. 5. The individual plots were initially segmented using the forest map provided by the Tomakomai forestry management [26], and then, the intensity moment was estimated and converted into biomass in each segmented plot. This is a typical example of what can be done by the moment model described in this letter.

Caution, however, should be made on the usage of the regression model derived in this letter that the texture information depends on the spatial resolution of SAR, and the intensity moment varies even for the same forests if the SAR resolution changes. Generally, increasing spatial resolution increases non-Gaussianity and corresponding intensity moment. The backscatter RCS depends on the radar incidence angles [27], [28], and therefore, the intensity moment is also expected to vary as the incidence angle changes. In the present analysis, the incidence angles changed from 40° to 47° at the near to far range in Fig. 1 so that the effect may be considered as small within the scene. As mentioned in our previous papers [15],

TABLE II
COMPARISON OF THE MODEL-BASED BIOMASS BY THE MOMENT METHOD ($M$-MODEL) AND THE GROUND-TRUTH BIOMASS FOR STANDS 20–40. THE BIOMASS IS IN THE UNIT OF TONS PER HECTARE

| stands | $M$-model | ground-truth | stands | $M$-model | ground-truth |
|---|---|---|---|---|---|
| 20 | 67.4 | 50.8 | 31 | 45.0 | 36.5 |
| 21 | 99.7 | 107.8 | 32 | 92.5 | 79.3 |
| 22 | 59.4 | 85.6 | 33 | 92.2 | 97.2 |
| 23 | 94.7 | 111.8 | 34 | 88.7 | 97.4 |
| 24 | 71.6 | 71.9 | 35 | 67.1 | 52.4 |
| 25 | 53.5 | 43.8 | 36 | 89.2 | 121.0 |
| 26 | 70.9 | 67.5 | 37 | 65.1 | 66.8 |
| 27 | 84.7 | 71.6 | 38 | 0.1 | 0.1 |
| 28 | 92.2 | 79.6 | 39 | 66.5 | 56.9 |
| 29 | 98.7 | 126.7 | 40 | 99.9 | 125.3 |
| 30 | 96.5 | 97.5 | | | |
| total | | | | 1645.6 | 1693.6 |
| average | | | | 74.8 | 77.0 |

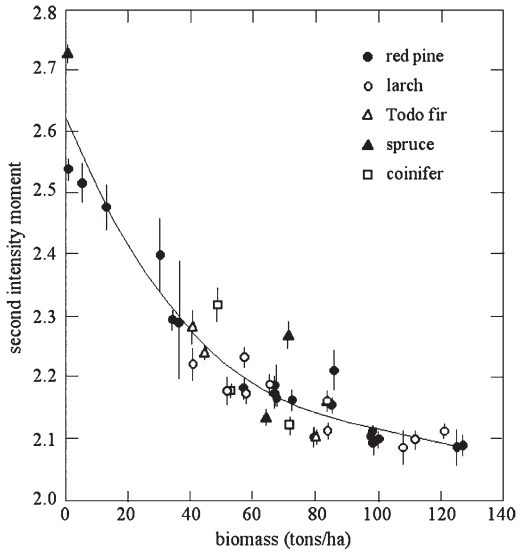


Fig. 4. Second intensity moment $\langle I^2 \rangle / \langle I \rangle^2$ of the cross-polarization data as a function of tree biomass of all stands 1–40.

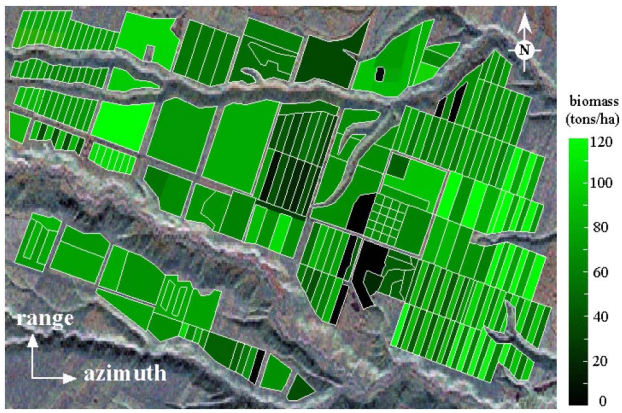


Fig. 5. Biomass map of the test site area in the Tomakomai national forests computed by using the moment model function from the L-band cross-polarization Pi-SAR data.

[16], in the situations of different spatial resolution, incidence angles, and slopes, the regression analysis needs to be taken again for the new sets of data. Nevertheless, the present study will certainly open a new and different approach to biomass estimation by high-resolution SAR.

## IV. Conclusion

A simple method has been described on the estimation of tree biomass of coniferous forests from the second intensity moment of high-resolution cross-polarized Pi-SAR L-band data over the Tomakomai national forests in Hokkaido, Japan. The technique is to utilize the model function computed from the regression analysis using the ground-truth biomass and the second intensity moment in the textured SAR images that obey non-Gaussian statistics. The regression model function was derived using the data of 19 stands, and comparison was made between the model-based biomass and the ground-truth biomass of other 21 sets of data, resulting in the average measurement accuracy of approximately 85%. A possible application of making a biomass map has also been presented. The moment model does not require any distribution function such as $K$-distribution. This method neither requires such strict calibration as for the RCS-based models. In this letter, the model function was derived from the coniferous forests in Hokkaido, Japan, but the technique can be applied to other forests with similar conditions.

## Acknowledgment

The authors would like to thank Dr. M. Shimada of JAXA for processing and providing the Pi-SAR data.

## References

[1] J. T. Houghton, L. G. M. Filho, D. J. Griggs, and K. Maskell, Eds., "Stabilization of atmospheric greenhouse gases: Physical, biological and socio-economic implications," in *IPCC Technical Paper III*. Cambridge, U.K.: Cambridge Univ. Press, Feb. 1997, p. 38.

[2] F. T. Ulaby, K. Sarabandi, K. McDonald, M. Whitt, and M. C. Dobson, "Michigan microwave canopy scattering model," *Int. J. Remote Sens.*, vol. 11, no. 7, pp. 1223–1253, Jul. 1990.

[3] Y. H. Hussin, R. M. Reich, and R. M. Hoffer, "Estimating slash pine biomass using radar backscatter," *IEEE Trans. Geosci. Remote Sens.*, vol. 29, no. 3, pp. 427–431, May 1991.

[4] M. C. Dobson, F. T. Ulaby, T. Le Toan, A. Beaudoin, E. S. Kasischke, and N. Christensen, "Dependence of radar backscatter on coniferous forest biomass," *IEEE Trans. Geosci. Remote Sens.*, vol. 30, no. 2, pp. 412–415, Mar. 1992.

[5] T. Le Toan, A. Beaudoin, J. Riom, and D. Guyon, "Relating forest biomass to SAR data," *IEEE Trans. Geosci. Remote Sens.*, vol. 30, no. 2, pp. 403–411, Mar. 1992.

[6] K. J. Ranson and Q. Sun, "Mapping biomass of a northern forest using multifrequency SAR data," *IEEE Trans. Geosci. Remote Sens.*, vol. 32, no. 2, pp. 388–396, Mar. 1994.

[7] Y. Rauste, T. Häme, J. Pulliainen, K. Heiska, and M. Hallikainen, "Radar-based forest biomass estimation," *Int. J. Remote Sens.*, vol. 15, no. 14, pp. 2797–2808, Sep. 1994.

[8] P. Ferrazzoli and L. Guerriero, "Radar sensitivity to tree geometry and woody volume: A model analysis," *IEEE Trans. Geosci. Remote Sens.*, vol. 33, no. 2, pp. 360–371, Mar. 1995.

[9] M. L. Imhoff, "Radar backscatter and biomass saturation: Ramifications for global biomass inventory," *IEEE Trans. Geosci. Remote Sens.*, vol. 33, no. 2, pp. 511–518, Mar. 1995.

[10] J. E. S. Fransson and H. Israelsson, "Estimation of stem volume in boreal forests using ERS-1 C- and JERS-1 L-band SAR data," *Int. J. Remote Sens.*, vol. 20, no. 1, pp. 123–137, Jan. 1999.

[11] Y. Rauste, "Multi-temporal JERS SAR data in boreal forest biomass mapping," *Remote Sens. Environ.*, vol. 97, no. 2, pp. 263–275, Jul. 2005.

[12] M. Watanabe, M. Shimada, A. Rosenqvist, T. Todono, M. Matsuoka, S. A. Romshoo, K. Ohita, R. Furuta, K. Nakamura, and T. Moriyama, "Forest structure dependency of the relation between L-band $\sigma^0$ and biophysical parameters," *IEEE Trans. Geosci. Remote Sens.*, vol. 44, no. 11, pp. 3154–3165, Nov. 2006.

[13] S. S. Saatchi, R. A. Houghton, R. C. Dos Santos Alvala, J. V. Soares, and Y. Yu, "Distribution of aboveground live biomass in the Amazon basin," *Global Change Biol.*, vol. 13, pp. 816–837, 2007.

[14] R. N. Treuhaft and P. R. Siqueira, "The calculated performance of forest structure and biomass estimates from interferometric radar," *Waves Random Media*, vol. 14, no. 2, pp. S345–S358, 2004.

[15] H. Wang and K. Ouchi, "Accuracy of the $K$-distribution regression model for forest biomass estimation by high-resolution polarimetric SAR: Comparison of model estimation and field data," *IEEE Trans. Geosci. Remote Sens.*, vol. 46, no. 4, pp. 1058–1064, Apr. 2008.

[16] H. Wang, K. Ouchi, M. Watanabe, M. Shimada, T. Tadono, A. Rosenqvist, S. A. Romshoo, M. Matsuoka, T. Moriyama, and S. Uratsuka, "In search of the statistical properties of high-resolution polarimetric SAR data for the measurements of forest biomass beyond the RCS saturation limits," *IEEE Geosci. Remote Sens. Lett.*, vol. 3, no. 4, pp. 495–499, Oct. 2006.

[17] C. J. Oliver and S. Quegan, *Understanding Synthetic Aperture Radar Images*. London, U.K.: Artech House, 1998.

[18] C. J. Oliver, "The interpretation and simulation of clutter textures in coherent images," *Inv. Probl.*, vol. 2, no. 4, pp. 481–518, Nov. 1986.

[19] E. Jakeman, "On the statistics of $K$-distributed noise," *J. Phys. A, Math. Gen.*, vol. 13, no. 1, pp. 31–48, Jan. 1980.

[20] T. Kobayashi, T. Umehara, M. Satake, A. Nadai, S. Uratsuka, T. Manabe, H. Masuko, M. Shimada, H. Shinohara, H. Tozuka, and M. Miyawaki, "Airborne dual-frequency polarimetric and interferometric SAR," *IEICE Trans. Commun.*, vol. E83-B, no. 9, pp. 1945–1954, Sep. 2000.

[21] F. T. Ulaby, F. Kouyate, B. Brisco, and T. H. L. Williams, "Textural information in SAR images," *IEEE Trans. Geosci. Remote Sens.*, vol. GRS-24, no. 2, pp. 235–245, Mar. 1986.

[22] L. Kurvonen and M. T. Hallikainen, "Textural information of multitemporal ERS-1 and JERS-1 SAR images with applications to land and forest type classification in boreal zone," *IEEE Trans. Geosci. Remote Sens.*, vol. 37, no. 2, pp. 680–689, Mar. 1999.

[23] C. J. Oliver, "Rain forest classification based on SAR texture," *IEEE Trans. Geosci. Remote Sens.*, vol. 38, no. 2, pp. 1095–1104, Mar. 2000.

[24] G. De Grandi, J.-S. Lee, D. Shuler, and E. Nezry, "Texture and speckle statistics in polarimetric SAR synthesized images," *IEEE Trans. Geosci. Remote Sens.*, vol. 41, no. 9, pp. 2070–2088, Sep. 2003.

[25] T. M. Kuplich, P. J. Curran, and P. M. Atkinson, "Relating SAR images texture to the biomass of regenerating tropical forests," *Int. J. Remote Sens.*, vol. 26, no. 21, pp. 4829–4854, Nov. 2005.

[26] Project department, Stand Volume Table -East Japan-, Japan Forestry Investigation Committee, Tokyo, Japan: Forestry Agency, Oct. 1998.

[27] S. S. Saatchi and K. C. McDonald, "Coherent effects in microwave backscattering models for forest canopies," *IEEE Trans. Geosci. Remote Sens.*, vol. 35, no. 4, pp. 1032–1044, Jul. 1997.

[28] Y. Rauste, "Incidence-angle dependence in forested and non-forested areas in Seasat SAR data," *Int. J. Remote Sens.*, vol. 11, no. 7, pp. 1267–1276, Jul. 1990.